Monthly Notices
of the
ROYAL ASTRONOMICAL SOCIETY

MNRAS **433,** 1300–1311 (2013)
Advance Access publication 2013 June 8

doi:10.1093/mnras/stt812

Apsidal motion in massive close binary systems – I. HD 165052, an extreme case?

G. Ferrero,[1,2]★† R. Gamen,[1,2]‡ O. Benvenuto[1,2]§ and E. Fernández-Lajús[1,2]

[1]*Facultad de Ciencias Astronómicas y Geofísicas, Universidad Nacional de La Plata, Paseo del Bosque S/N, 1900 La Plata, Argentina*
[2]*Instituto de Astrofísica de La Plata, CCT La Plata–CONICET, UNLP, Argentina*

Accepted 2013 May 7. Received 2013 May 4; in original form 2013 March 11

ABSTRACT

We present a new set of radial velocity measurements of the spectroscopic binary HD 165052 obtained by disentangling high-resolution optical spectra. The longitude of the periastron ($\varpi = 60 \pm 2^\circ$) shows a variation with respect to previous studies. We have determined the apsidal motion rate of the system, $\dot{\varpi} = 12.1 \pm 0.^\circ3$ yr^{-1}, which was used to calculate the absolute masses of the binary components: $M_1 = 22.5 \pm 1.0\,\mathrm{M}_\odot$ and $M_2 = 20.5 \pm 0.9\,\mathrm{M}_\odot$. Analysing the separated spectra, we have reclassified the components as O7Vz and O7.5Vz stars.

Key words: binaries: close – binaries: spectroscopic – stars: early-type – stars: fundamental parameters – stars: individual: HD 165052 – stars: massive.

1 INTRODUCTION

O-type stars are objects that deserve great astrophysical interest. Usually, they are located in star-forming regions where, due to their high-velocity winds and intense ultraviolet radiation, they determine the dynamical and ionization state of the neighbouring interstellar medium. The turbulence they generate in the interstellar medium drives galactic dynamos. Furthermore, their high luminosities dominate the radiation of their birth regions, open clusters, spiral arms and even entire galaxies. Additionally, by mean of their explosive end as supernovae, they play a key role in the chemical evolution of the interstellar medium and therefore in the metal enrichment of successive generations of stars. However, several features of O-type stars are still poorly known. In particular, the mass of an O-type star represents a fundamental astrophysical parameter, which is still highly uncertain for various spectral subtypes. For this reason, to establish constraints on the masses of O-type stars is a very important task. The most direct and reliable method of determining stellar masses is analysis of the Keplerian motion in detached double-lined eclipsing binary systems. Photometric and spectroscopic observation of such systems, and subsequent analysis of the variations in their brightness and radial velocities (RV), allows one to calculate the parameters of their orbital motion and the minimum masses of their components. Furthermore, the observation of eclipses indicates that the orbital plane lies close to the line of sight (i. e. its inclination i is close to 90°). Then, using adequate models of stellar structure, it is possible to derive absolute stellar masses. However, it should be emphasized that this can be done only for a very limited number of systems, since the constraint $i \sim 90^\circ$ is quite strong.

In close binaries, due to the proximity of the companion the stars are no longer spherical. This leads to the occurrence of finite quadrupolar and higher momenta of the gravitational field (cf. Sterne 1939). These momenta force eccentric orbits to precess, i.e. to modify the position of periastron (apside or apse). Additionally, general relativity predicts a secular apsidal motion, which is independent of the classical contributions but is again related to the masses of the components (cf. Levi-Civita 1937). It has been shown that knowledge of the apsidal motion rate (AMR) allows one to estimate absolute masses in massive close binary systems with unknown orbital inclination even in the case of non-eclipsing binaries (Benvenuto et al. 2002, hereafter B02). From a theoretical point of view, the AMR is strongly dependent on the radii and internal structure of the stars of the pair. Thus, the masses determined by this method will be model-dependent. In any case, accurate RV measurements and improved stellar evolutionary models currently make its use feasible in reliable mass determinations. In order to increase the number of O-type stars with determined absolute masses, we are conducting a systematic high-resolution spectroscopic monitoring of binary systems with eccentric orbits with the aim of calculating their masses by taking advantage of this method.

One of the objects that we are studying is HD 165052 (= CD −24 13864: $\alpha_{2000} = 18^\mathrm{h}05^\mathrm{m}10.^\mathrm{s}6$, $\delta_{2000} = -24^\circ23'55''$; $V = 6.87$), an O-type double-lined spectroscopic binary star member of the open cluster NGC 6530 in the H II region M8 (the Lagoon Nebula). It was first catalogued in the Cordoba Durchmusterung

★E-mail: gferrero@fcaglp.unlp.edu.ar
† Visiting Astronomer, CASLEO (operated under agreement between the Consejo Nacional de Investigaciones Científicas y Técnicas de la República Argentina and the National Universities of La Plata, Córdoba and San Juan).
‡ Visiting Astronomer, LCO.
§ Member of the Carrera del Investigador Científico, Comisión de Investigaciones Científicas de la Provincia de Buenos Aires, La Plata, Argentina.

Table 1. Technical characteristics of the instruments in the configurations used for this work.

Telescope–instrument	Reciprocal dispersion (Å/pixel)	R @5000 Å	Spectral range (Å)
CASLEO–J.S.–REOSC	0.19	13 000	3600–6100
ESO–2.2–FEROS	0.03	45 000	3600–9200
LCO–du Pont–Echelle	0.05	35 000	3500–10100

by Thome (1892). Plaskett (1924) discovered variations in the RV of this star, while double lines in its spectrum were first noticed by Conti (1974). Morrison & Conti (1978) presented the first orbital solution for the system. An improved circular orbital solution was calculated by Stickland, Lloyd & Koch (1997, hereafter S97) adding RV measurements from *International Ultraviolet Explorer* (*IUE*) spectra. A few years later, Arias et al. (2002, hereafter A02) analysed high-resolution optical spectra and determined a slightly eccentric ($e = 0.09$) orbital solution. They fitted the previous RV data with their own solution and found evidence of apsidal motion. Linder et al. (2007, hereafter L07) determined a new orbital solution for the system that agrees with the A02 one.

In order to establish (or rule out) the AMR in HD 165052, we have systematically observed this star between 2008 and 2010 and gathered a set of high-resolution spectra (see Section 2). Using the technique of disentangling (cf. González & Levato 2006), we have measured the RVs and simultaneously obtained separated spectra of the two components of the binary (see Section 3.1). This procedure allowed us to reclassify the spectra of both components (Section 3.2) and to fit a new orbital solution (Section 3.4). We have confirmed the existence of apsidal motion and measured the AMR for the first time (Section 3.5). Then, applying the method mentioned above (B02), we have calculated the masses of the system components (Section 3.6).

2 OBSERVATIONS

We have acquired 37 high-resolution spectra of HD 165052: 29 at Complejo Astronómico El Leoncito (CASLEO), Argentina, with the 2.15-m Jorge Sahade telescope between 2008 August and 2010 August using the Recherches et Études d'Optique et de Sciences Connexes Spectrograph Echelle Liège (REOSC SEL)[1] Cassegrain spectrograph in cross-dispersion mode; 5 at Las Campanas Observatory (LCO), Chile, with the Irénée du Pont 2.5-m telescope using the Echelle Spectrograph in May 2010; and 3 additional spectra using the Fibre-fed, Extended Range, Échelle Spectrograph (FEROS) at ESO La Silla, Chile, with the 2.2-m telescope in 2009 May. The spectra taken at LCO and ESO La Silla belong to the 'OWN Survey' programme (Barbá et al. 2010). The mean signal-to-noise ratio (SNR) of all these spectra is ∼200. Technical details of the instrumental configurations can be found in Table 1. All the spectra were reduced using the standard routines of IRAF.[2]

At CASLEO every night we took at least one spectrum of the star HD 137066, a RV standard established using the Correlation Radial Velocities (CORAVEL) photoelectric scanner by Andersen et al. (1985), with $v_r = -8.72 \pm 0.15$ km s^{-1}. We have also observed the B0V star τ Sco, considered as a rotational velocity standard in the Slettebak et al. (1975) system with $v \sin i < 10$ km s^{-1}. The latter spectra were taken with the same instrumental configuration as those of HD 165052 and averaged to achieve SNR $\gtrsim 600$ in the region of interest.

Spectra from CASLEO and LCO were calibrated using comparison spectra taken after every single exposition from a Th–Ar lamp.

3 RESULTS AND DISCUSSION

3.1 Disentangling and radial velocity measurements

In order to measure the RVs, we applied the disentangling method described by González & Levato (2006), which allows one to separate the spectra of the binary components simultaneously. This iterative procedure consists of alternately using the spectrum of one component to calculate the spectrum of the other. In each step, the spectrum of one star is used to subtract its spectral features from the composite one. Then, the RVs are measured in the resulting single-lined spectra. These spectra are shifted appropriately and combined to compute the new spectrum of each component.

We have started the iterations using a template spectrum of the secondary star taken from the grid of stellar atmosphere models in the TLUSTY data base (Lanz & Hubeny 2003) with solar metallicity,[3] $T_{\rm eff,\,2} = 35\,000$ K and $\log g_2 = 4.0$, which corresponds to a main-sequence star (cf. Section 3.2). The $T_{\rm eff}$ was chosen adopting the spectral type calibration of Martins, Schaerer & Hillier (2005). The template was convolved to the projected rotational velocity estimated by Morrison & Conti (1978). As has been shown by González & Levato (2006), these initial guesses do not affect the final results.

The method also requires a RV initial value for each spectrum. A first raw measurement of the central wavelengths of the spectral lines He I λλ4471, 4921, 5876, He II λλ4686 and 5411 was made using the SPLOT task of IRAF. The RVs calculated from these lines were averaged to obtain a first estimate of the RV of each component. Instead, during disentangling iterations the cross-correlation function was calculated over a disjoint sample region composed of 17 wavelength intervals, each ∼10 Å wide, taken around the following spectral lines: He I λλ3819, 4026, 4387, 4471, 4713, 4921, 5015, 5875; He II λλ4200, 4542, 4686, 5411; C IV λλ5801, 5812; O III λ5592; Mg II λ4481; Si IV λ4088. The RVs thereby measured are listed in Table 2 and reproduced as *mean* RVs in Table B2.[4]

In order to provide detailed data for future works, we have subsequently defined several sampling regions, each one around a single spectral line, and computed the cross-correlation separately for each region. We have therefore measured the RVs of the individual lines listed in Table B2. The spectral lines selected were the same as those of A02, to allow for a comparison with that work. As can be seen in Appendix B, the overall behaviour of the RVs of the individual lines agrees with that of the *mean* RV.

[1] Jointly built by REOSC and Liège Observatory and on a long-term loan from the latter.

[2] IRAF is distributed by the National Optical Astronomy Observatories, which are operated by the Association of Universities for Research in Astronomy, Inc., under cooperative agreement with the National Science Foundation.

[3] From here on, subscripts 1 and 2 will identify the stellar parameters of the primary and secondary component of the system, respectively.

[4] Table B2 is also available in electronic form at the Centre de Donnes astronomiques de Strasbourg (CDS) at http://vizier.u-strasbg.fr/viz-bin/VizieR.

Table 2. Journal of the observations of HD 165052. Radial velocity measurements are used to compute the orbital solution given in Table 3.

HJD −245 0000	Phase ϕ	v_1	O–C	v_2	O–C	Obs.
4582.8675	0.90	97.1	−2.6	−108.8	−2.4	CAS
4693.6231	0.38	−81.6	3.2	91.7	−3.9	CAS
4695.6483	0.06	13.8	0.9	−8.8	2.6	CAS[a]
4696.5568	0.37	−85.4	0.8	95.1	−1.9	CAS
4696.6286	0.39	−80.2	0.9	94.3	2.8	CAS
4696.6605	0.40	−76.8	1.6	91.4	2.8	CAS
4697.6220	0.73	73.7	2.9	−76.1	−1.4	CAS
4955.8004	0.10	−7.6	5.3	5.1	−11.7	ESO[a]
4956.9100	0.47	−57.5	−2.4	61.0	−2.0	ESO
4964.8865	0.17	−57.6	0.5	66.7	0.4	CAS
4965.8323	0.49	−47.1	0.0	57.4	3.2	CAS
4966.8550	0.84	100.8	−1.4	−106.1	2.9	CAS
4967.8220	0.16	−56.1	−1.3	62.9	0.2	CAS
4968.8723	0.52	−38.8	−4.6	40.5	0.5	CAS
5046.6533	0.84	103.7	1.3	−109.9	−0.5	CAS
5047.7305	0.21	−73.8	−0.7	81.8	−1.0	CAS
5048.7185	0.54	−24.6	−0.2	29.3	−0.2	CAS[a]
5049.7159	0.88	106.4	4.3	−106.5	2.5	CAS
5052.7320	0.90	100.6	1.5	−104.9	0.8	CAS
5337.6475	0.31	−94.3	−2.8	101.3	−1.6	LCO
5339.7307	0.02	38.0	−3.8	−45.7	−2.7	LCO
5340.6327	0.33	−94.6	−3.4	100.7	−1.8	LCO
5341.5812	0.65	26.4	−3.8	−27.4	2.9	LCO[a]
5342.6292	0.00	54.0	−0.5	−60.9	−4.0	LCO
5376.5522	0.48	−52.2	−0.3	59.9	0.4	CAS
5378.7551	0.23	−79.7	0.0	88.5	−1.4	CAS
5380.5253	0.82	97.3	−3.3	−106.1	1.2	CAS
5381.7473	0.24	−84.7	−1.7	93.2	−0.4	CAS
5383.7515	0.92	91.5	−3.2	−98.5	2.5	CAS
5429.6974	0.46	−57.0	1.1	70.1	3.8	CAS
5430.6168	0.78	87.8	−1.1	−91.7	2.9	CAS
5431.6959	0.14	−42.6	−1.1	51.4	3.2	CAS
5432.6362	0.46	−58.1	2.1	69.5	0.9	CAS
5433.5059	0.75	81.0	0.0	−88.3	−2.4	CAS
5434.6834	0.15	−46.7	1.2	61.2	6.1	CAS
5435.5627	0.45	−65.0	−1.2	74.0	1.4	CAS
5698.8397	0.54	−6.0	17.1	41.2	13.2	ESO[a]

Notes. Velocities and O–C in km s^{-1}.
[a]One tenth weight assigned in orbital solution fit because of strong lines blending.
Obs. – observatory where the spectrum was acquired. CAS: CASLEO; ESO: ESO La Silla; LCO: Las Campanas.

3.2 Spectral analysis

We have visually compared our disentangled spectra with those of the atlas of spectral standards published by Sota et al. (2011) using the MGB code (Maíz Apellániz et al. 2011). We have observed in both components that the intensity of the absorption line He II λ4686 is greater than both He I λ4471 and He II λ4542 (see Fig. A1), a fact that is noted with a *z* qualifier of the spectral type (cf. Walborn 2009). Thus we classified the primary as O7V*z* and the secondary as O7.5V*z*.

In the past, other authors have classified these stars spectroscopically. Morrison & Conti (1978) observed that both stars are normal, with no conspicuous mass loss, and not far from the zero-age main sequence (ZAMS). A02 showed that the spectral types are O6.5V for the primary component and O7.5V for the secondary. L07 concluded that the system could be O6.5V + O7V or O6.5V + O7.5V, perhaps O((f)), because they detected N III λλ4634, 40 and 41 in emission. We see some traces of very weak emission around 4640 in a couple of FEROS spectra. In our disentangled primary-component spectrum, the absorption lines He I λ4471 and He II λ4542 seem to have almost the same intensity. That is why we suspect it could be an O7V rather than an O6.5V star. For the classification of the secondary, we agree with the spectral type proposed by A02 and L07.

3.3 Projected rotational velocity

One of the stellar parameters required for mass determination is the projected rotational velocity $v \sin i$ of the binary components, since it is used to compute the internal structure constants (see Section 3.6).

To estimate $v \sin i$, the spectrum of τ Sco has been convolved with rotation-line profiles calculated for different projected rotational velocities. The He I λλ4713 and 5015 absorption lines were selected for these measurements because they are isolated in the spectra and their Stark broadening can be considered as negligible (cf. Dimitrijevic & Sahal-Brechot 1990). The full widths at half-maximum of intensity (FWHM) of these lines in the convolved spectra of τ Sco were measured and a linear relation between FWHM and $v \sin i$ was fitted supposing a rotational velocity much lower than the critical one (cf. Collins 1974). Specifically, we found $\mathrm{FWHM}_{4713} = 0.0228 \times v \sin i + 0.219$ and $\mathrm{FWHM}_{5015} = 0.0239 \times v \sin i + 0.277$ Å, in the interval $30 \leq v \sin i \leq 100$ km s^{-1}. These empirical regressions were used to convert the FWHM of each line measured in the disentangled spectra into a $v \sin i$ value.

Thereby we have computed $v_1 \sin i = 71 \pm 5$ km s^{-1} and $v_2 \sin i = 66 \pm 5$ km s^{-1}, where the errors were estimated as half the uncertainty in the projected rotational velocity of τ Sco.

Other authors have estimated the $v \sin i$ of these stars: from *IUE* spectra, S97 have found $v_1 \sin i = 85 \pm 8$ and $v_2 \sin i = 80 \pm 6$ km s^{-1}; from the FWHM intensity of the individual profiles of He I λ4471, Morrison & Conti (1978) have obtained $v_1 \sin i = 65 \pm 9$ and $v_2 \sin i = 69 \pm 4$ km s^{-1}; L07 determined $v_1 \sin i = 73 \pm 7$ and $v_2 \sin i = 80 \pm 7$ km s^{-1} using the profiles of the disentangled lines He II λ4471, He II λ4542 and Hβ. From the four independent determinations, it is clear that the projected rotation velocity of both stars is very similar (within errors). Our results compare better with the later ones.

3.4 Orbital solution

Our orbital solution was obtained using the RVs given in Table 2 as input for the GBART[5] code. The orbital parameters determined from the best fit are shown in the last column of Table 3 and depicted in Fig. 1. Our new orbital solution is close to the already published ones by S97, A02 and L07; the latter discussed the comparisons among these. We also found a non-negligible eccentricity, thus confirming its reliability. However, we point out the noticeable difference in the periastron longitudes (ϖ), a clear sign of apsidal motion, which will be analysed in the following subsection.

3.5 Apsidal motion

Our orbital solution (Table 2) gives $\varpi = 60 \pm 2^\circ$, a very different value from those found by A02 and L07, two solutions based on

[5] Based on the algorithm of Bertiau & Grobben (1969) and implemented by F. Bareilles (available at http://www.iar.unlp.edu.ar/~fede/pub/gbart).

Table 3. Orbital solutions previously published for HD 165052, for comparison with this work.

Element	M78	S97	A02	L07	This work
P (days)	6.140 ± 0.002	2.955055	2.95510 ± 0.00001	2.95515 ± 0.00004	2.95506 ± 0.00002
e	0.064 ± 0.041	0.0 (assumed)	0.09 ± 0.004	0.081 ± 0.015	0.090 ± 0.003
$\varpi(^\circ)$	304 ± 56^a	undefined	296.7 ± 3.5	298.0 ± 10.2	60 ± 2
T_0 (HJD −240 0000)	42939.5 ± 0.6	49819.075 ± 0.008	49871.75 ± 0.03	51299.053 ± 0.081	55050.08 ± 0.02
$TV_{\max}$ (HJD −240 0000)			49872.19 ± 0.03		55049.66 ± 0.02
V_0 (km s^{-1})	3.0 ± 4.6	-0.9 ± 1.3	1.05 ± 0.31	2.1 ± 1.2^c	1.3 ± 0.2
K_1 (km s^{-1})	91.0 ± 2.8	95.6 ± 2.2	94.8 ± 0.5	96.4 ± 1.6	97.4 ± 0.4
K_2 (km s^{-1})	104.0 ± 8.6	109.6 ± 2.2	104.7 ± 0.5	113.5 ± 1.9	106.5 ± 0.4
$a_1 \sin i$ ($R_\odot$)	11.1 ± 0.3	5.58 ± 0.13	5.51 ± 0.03	5.6 ± 0.1	5.66 ± 0.03
$a_2 \sin i$ ($R_\odot$)	12.7 ± 0.7	6.40 ± 0.13	6.09 ± 0.03	6.6 ± 0.1	6.20 ± 0.03
$M_1 \sin^3 i$ ($M_\odot$)	2.5 ± 0.5	1.41 ± 0.07	1.26 ± 0.03	1.5 ± 0.1	1.34 ± 0.03
$M_2 \sin^3 i$ ($M_\odot$)	2.2 ± 0.3	2.23 ± 0.06^b	1.14 ± 0.03	1.3 ± 0.1	1.22 ± 0.03
$q(M_2/M_1)$	0.87 ± 0.08	0.87 ± 0.03	0.90 ± 0.01	0.85 ± 0.01	0.91 ± 0.01
r.m.s. (km s^{-1})		7.4	2.21	6.2	1.7

Notes. M78: Morrison & Conti (1978); S97: Stickland et al. (1997); A02: Arias et al. (2002); L07: Linder et al. (2007).
[a]Measured from maximum positive radial velocity of star 1.
[b]It seems that there was a typing mistake in this article. The mass should probably be 1.23 $M_\odot$.
[c]L07 fitted considering possible different systemic velocities for both components. The listed value corresponds to the primary. For the secondary they found 1.4 ± 1.3 km s^{-1}.

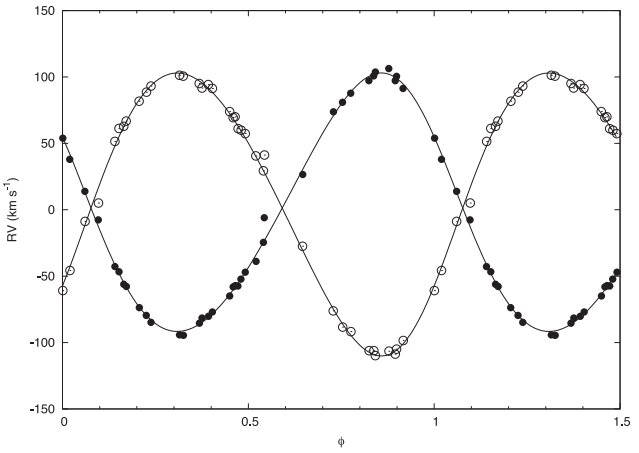

Figure 1. Radial velocity curve of HD 165052 calculated with the ephemerides of the orbital solution found in this work (Table 3). Measurements from Table 2 are also represented (filled circles: primary radial velocities; open: secondary). $\phi = 0$ corresponds to the periastron passage.

observations overlapped in time. We consider that this variation confirms the existence of apsidal motion in the system. To determine its rate, we have re-computed orbital solutions to the previously published RVs, fixing $P = 2.95506$ d and $e = 0.090$ (note that our values for these parameters do not differ significantly from those of S97, A02 and L07). To do this, we have grouped those data into four data sets according to the proximity of the observation date (see Table 4). This means that we have joined together the data from A02 and L07, while we have not taken into account four data points from S97 between HJD 244 4121.777 and 244 5123.793. It is worth noting that the zero-point in RV does not vary, within errors, between the different data sets. We have considered each ϖ_i thus obtained as representative of the longitude of the periastron at an epoch t_i equal to the mid-point time between the first and the last date of the observations in that particular data set. Since the variation of ϖ in time seems to have a linear trend (see Fig. 2) we have computed a linear regression, the slope of which was considered as a first approximation to the AMR of the system:

$$\dot{\varpi} = 0.0322 \pm 0.^\circ0005 \text{ day}^{-1}. \quad (1)$$

Table 4. Longitude of the periastron ϖ and other orbital elements at different epochs recomputed from previously published RV measurements, fixing $P = 2.95506$ d and $e = 0.090$.

Data set no.	1	2	3	4
Initial date (HJD −240 0000)	42560.940	48864.018	49854.6400	54582.8675
Final date (HJD −240 0000)	43092.571	49965.110	52383.8577	55698.8397
Data from	M78	S97	A02, L07	This work
$\varpi(^\circ)$	27 ± 22	247 ± 9	293 ± 4	60 ± 2
V_0 (km s^{-1})	0 ± 2	-1.7 ± 0.9	1.3 ± 0.4	1.3 ± 0.2
K_1 (km s^{-1})	94 ± 4	97 ± 2	95.4 ± 0.8	97.4 ± 0.4
K_2 (km s^{-1})	103 ± 4	106 ± 2	107.8 ± 0.8	106.5 ± 0.4
q	0.91 ± 0.07	0.91 ± 0.03	0.89 ± 0.01	0.91 ± 0.01
r.m.s. (km s^{-1})	8.4	3.2	4.1	1.7

Note. References as in Table 3.

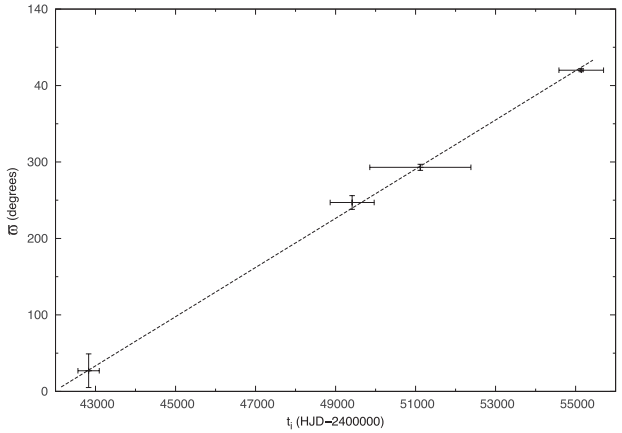

Figure 2. Variation of the longitude of the periastron (ϖ) in time. Horizontal error bars indicates the time span of each observational data set. A linear fit with slope $0.0322 \pm 0.^{\circ}0005$ day^{-1} is shown (data from Table 4).

We have also used the FOTEL code developed by Hadrava (2004), which allows one to solve a RV curve taking into account the apsidal motion. We have applied FOTEL to all the available RVs (Table B1) using as initial values our set of orbital parameters (Table 3, col. 'This work') and the $\dot{\varpi}$ value just obtained. Permitting the code to fit all parameters simultaneously, the fitting process converged to a set of orbital elements that agrees, within errors, with the values determined using the individual data sets. The AMR thus obtained was

$$\dot{\varpi} = 0.0340 \pm 0.^{\circ}0007 \text{ day}^{-1}. \quad (2)$$

In the following calculations we have used for AMR the value

$$\dot{\varpi} = 0.0331 \pm 0.^{\circ}0009 \text{ day}^{-1}, \quad (3)$$

since it is the mean between (1) and (2), while we have adopted as its error the semi-difference between them. (This AMR corresponds to $12.1 \pm 0.^{\circ}3$ yr^{-1}, or alternatively to an apsidal period $U = 29.8 \pm 0.8$ yr.) It seems to be the highest AMR ever measured in an O+O system, with the possible exception of DH Cep (HD 215835), the AMR of which has still to be confirmed (cf. Petrova & Orlov 1999; Bulut & Demircan 2007, and references therein).

3.6 Calculation of the masses of the system employing the advance of the apside

As stated above (see Section 1), the measurement of the secular advancement of the apside allows for the determination of the masses of the components of the system even for the case of non-eclipsing binaries. The method to be employed below has been proposed and applied for the massive, non-eclipsing binary HD 93205 by B02 (see also Jeffery 1984).

As is well known, the gravitational potential of each component of the pair is affected by the presence of the other star and also by its own rotation. If we consider only the lowest (quadrupolar) correction to the gravitational potential of each object, the theoretical advancement of the apside is given by equation (14) of Sterne (1939):

$$\frac{\dot{\varpi}}{\Omega_{\rm orbit}} = k_{2,1}\left(\frac{a_1}{A}\right)^5\left[15\frac{M_2}{M_1}f_2(e) + \frac{\omega_1^2 A^3}{GM_1}g_2(e)\right] + k_{2,2}\left(\frac{a_2}{A}\right)^5\left[15\frac{M_1}{M_2}f_2(e) + \frac{\omega_2^2 A^3}{GM_2}g_2(e)\right]. \quad (4)$$

Here $\dot{\varpi}$ is the AMR; $\Omega_{\rm orbit}$ denotes the mean orbital angular velocity; $k_{i,j}$ are the internal structure constants for the ith multipolar term of the potential expansion (here $i = 2$) and j denotes the component of the pair (see below for details); G is the gravitational constant; A is the semi-axis of the relative orbit; M_i, a_i, ω_i are the mass, mean radius and angular rotation velocity of the ith star respectively. $f_2(e)$ and $g_2(e)$ are functions of the eccentricity e, given by

$$f_2(e) = \frac{1 + \frac{3}{2}e^2 + \frac{3}{8}e^4}{(1-e^2)^5} \quad (5)$$

and

$$g_2(e) = \frac{1}{(1-e^2)^2}. \quad (6)$$

The first and second terms of the right-hand side (r.h.s.) of equation (4) correspond to the contributions due to the primary and secondary stars, respectively. In each of these terms, the first term in the bracket is due to the tidal effect of one star on the other while the second one is due to stellar rotation.

$$\frac{\dot{\varpi}_{\rm GR}}{\Omega_{\rm orbit}} = 6.36 \times 10^{-6}\frac{M_1 + M_2}{A(1-e^2)}, \quad (7)$$

where masses and A are in solar units. The internal structure constants $k_{i,j}$ are dependent on the structure of the stars. Most stellar evolution codes assume spherical symmetry, ignoring rotation. However, the departure from sphericity due to rotation modifies $k_{i,j}$ appreciably. Fortunately, Claret (1999) has shown that accounting for this correction is very simple, at least for $i = 2$. If we define $[k_{2,j}]_{\rm sph}$ as the internal structure constant corresponding to a spherical star, the corrected value of $k_{i,j}$ is given by

$$\log k_{2,j} = \log[k_{2,j}]_{\rm sph} - 0.87\frac{2\,V_j^2}{3g_j a_j}, \quad (8)$$

where V_j is the tangential velocity and g_j the surface gravitational acceleration. We shall consider

$$\frac{\dot{\varpi}}{\Omega_{\rm orbit}} + \frac{\dot{\varpi}_{\rm GR}}{\Omega_{\rm orbit}} = \frac{\dot{\varpi}_{\rm obs}}{\Omega_{\rm orbit}} \quad (9)$$

as an equation for M_1 as described in B02, where the reader will find further details on the method. As discussed there, this method is model-dependent, because $k_{i,j}$ evolves due to changes in the density profile of the star and, more importantly, a_j also evolves. Notice the steep dependence of equation (4) with the value of a_j. Thus, as a matter of fact, this method is *age-dependent*.

In order to apply the above-described method, we consider that both stars have the same age and are still burning hydrogen in their cores, as is indicated by the spectral classification. We have computed solar-composition stellar models with masses from 15–40 $M_\odot$ during core hydrogen burning in steps of 0.5 $M_\odot$. These models include mass loss, as in de Jager, Nieuwenhuijzen & van der Hucht (1988), and overshooting, as in Demarque et al. (2004); the rest of the code corresponds to that described by Benvenuto & De Vito (2003) for binary evolution.

We show in Fig. 3 the Hertzsprung–Russell (H–R) diagram for stellar masses in the range corresponding to the components of the pair, with the evolutionary tracks calculated using these models. We set stellar ages to zero on the ZAMS.

Also, we have computed the coefficient $k_{2,j}$, the evolution of which for different values of the initial mass is shown in Fig. 4, together with $k_{2,j}(R/R_\odot)^5$, which appears in equation (4). Now, we are in a position to employ the secular advancement of the apside ($\Omega_{\rm apse} \equiv \dot{\varpi}$) to determine the mass of the primary. A comparison of

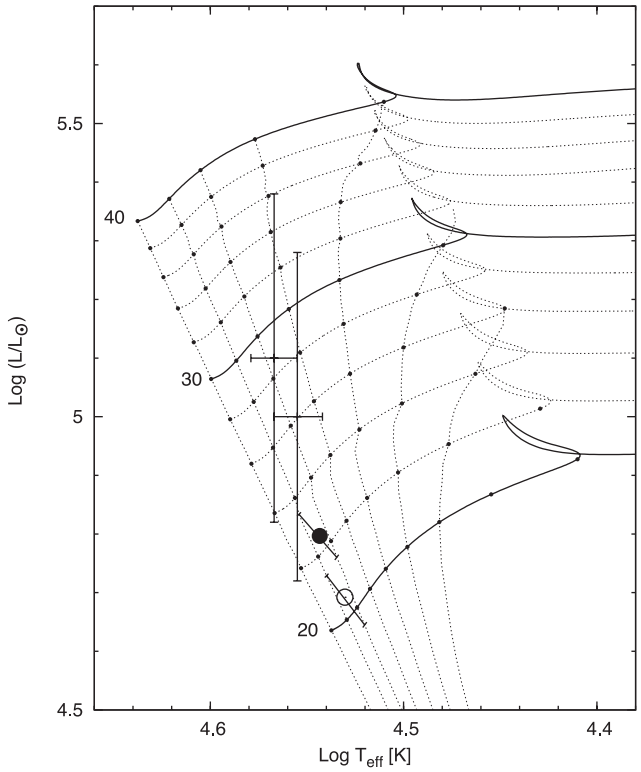

Figure 3. Evolutionary tracks in the H–R diagram for stars of 20, 30 and 40 $M_\odot$ (solid lines) and 22, 24, 26, 28, 32, 34, 36 and 38 $M_\odot$ (dotted lines) during core hydrogen burning. On each track, filled dots indicate time intervals of 1 Myr. Crosses: location of binary components according to the literature. Horizontal error bars: $T_{\rm eff}$ dispersion in the observational calibration of Martins et al. (2005, table 4). Vertical bars, lower limit: distance modulus from Mayne & Naylor (2008); upper limit: M_V from Buscombe (1969) (see details in Section 3.7). Circles: components derived from apsidal motion rate (filled primary); error bars depict the age uncertainty propagated to masses.

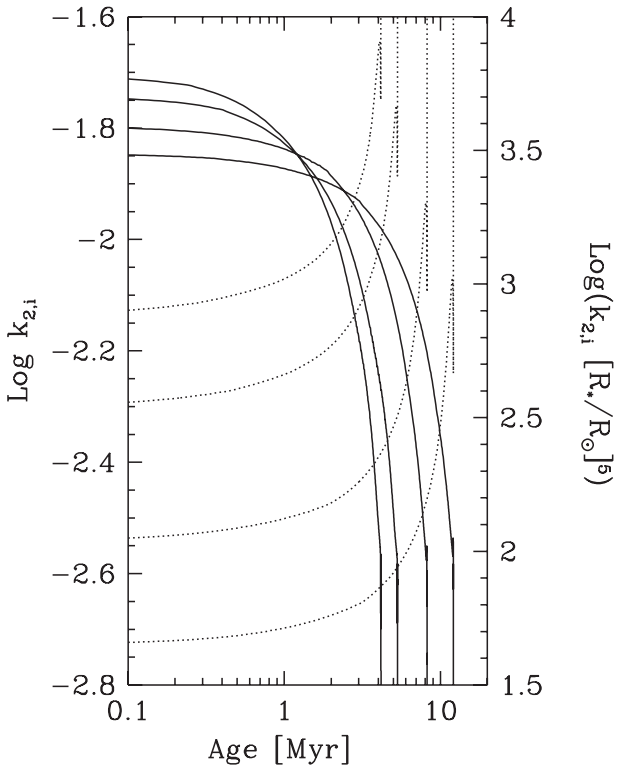

Figure 4. Temporal evolution of the coefficients $k_{2,j}$ (solid lines) and $k_{2,j}(R/R_\odot)^5$ (dotted lines) for stars of 15, 20, 30 and 40 $M_\odot$. Curves end at larger ages for smaller mass. For further details see Section 3.6.

the theoretical results with observations is presented in Fig. 5. For a given age of the pair, the mass value of the primary corresponds to the intersection of the theoretical curve with the horizontal line at $\Omega_{\rm apse}/\Omega_{\rm orbit} = (2.72 \pm 0.08) \times 10^{-4}$. The advancement of the apside is due to ≈74, ≈23 and ≈3 per cent tidal, rotational and relativistic contributions, respectively.

If we assume that the age of NGC 6530 is 1.5 Myr (see Section 3.7), the most probable mass value for the primary of HD 165052 is $22.5 \pm 1.0\,M_\odot$, where the error was estimated considering an age uncertainty of 0.5 Myr. Using the binary mass ratio q from our orbital solution, we found that the most probable value for the mass of the secondary is $M_2 = 20.5 \pm 0.9\,M_\odot$.

As HD 165052 is a much closer pair than HD 93205, it is worth analysing the possibility of considering contributions to the apsidal motion due to terms beyond the quadrupolar. These contributions have been given by Sterne (1939). It is found that the next term in the expansion for the advancement of the apside is approximately

$$2\frac{k_{3,j}}{k_{2,j}}\left(\frac{a_j}{A}\right)^2 \qquad (10)$$

times the tidal term considered in equation (4). Considering the solution given by equation (9), we find that $a_j/A \approx 1/3$, whereas the ratio of the internal structure constants can be estimated by employing table 15 of Claret & Gimenez (1991), corresponding to a stellar model of 25 $M_\odot$. It is found that $k_{3,j}/k_{2,j} \approx 1/3$. Thus, the correction due to the first term beyond the quadrupolar one is of the order of 4 per cent. This is far smaller than the uncertainty in the theoretical AMR due to an error of 0.5 Myr in the age of the pair. This fact justifies the employment of equation (4) up to the lowest-order contribution.

The component masses that we have obtained are in agreement, within errors, with the spectroscopic masses derived by Martins et al. (2005) from a $T_{\rm eff}$ calibration of O stars. In fact, they obtained $25.3\,M_\odot$ for an O7V star and $22.9\,M_\odot$ for an O7.5V with an uncertainty as high as 35–50 per cent. On the other hand, the masses calculated are close to the range of masses most reliably determined via detached eclipsing binaries for these spectral types. For example, the O7V stars V572 Car (= Tr16 104), primary, and HD 165921 (V3903 Sgr), primary, have masses of $23.5 \pm 0.1\,M_\odot$ and $27.27 \pm 0.55\,M_\odot$ respectively (cf. Vaz et al. 1997; Fernández Lajús 2006).

Nevertheless, the mass values we have derived from the apsidal motion rate are smaller than those estimated from photometric measurements and evolutionary tracks. We suspect that this difference should be mainly due to the large dispersion in the distance determinations of NGC 6530 found in the literature and probably also to the known mass discrepancy problem of O stars (cf. Massey et al. 2012). Even so, when we plot on the H–R diagram (Fig. 3) the points corresponding to our evolutionary models for the age assumed and the masses calculated, we find that they are consistent with the luminosities calculated from the most recent determinations of the cluster distance.

Additionally, the inclination of the orbit could be estimated from our mass determination. Taking the $M_1 \sin^3 i$ value from our orbital solution (Table 3), we derived $i \approx 23^\circ$, a result consistent with the fact that eclipses have never been reported.

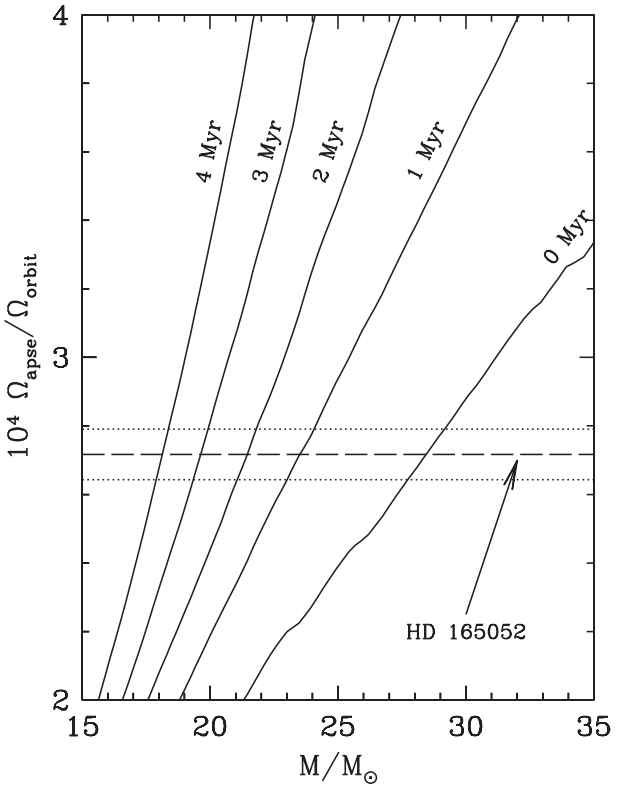

Figure 5. The secular advance of the apse as a function of the mass of the primary component of HD 165052 for different values of the age of the system, depicted by solid lines. The value corresponding to observations is denoted with a horizontal long dashed line. The value of the mass of the primary corresponds to the intersections: for ages of 0, 1, 2, 3 and 4 Myr, the values for the mass of the primary are of 28.4 ± 0.7, 23.5 ± 0.5, 21.5 ± 0.4, 19.6 ± 0.3 and $18.1 \pm 0.3\,M_\odot$, respectively. Evidently, the uncertainty in the age of the system has a direct impact on the determination of the masses of the components of the system.

The employed model is also capable of determining the radii of the components, giving $R_1 \sim 7\,R_\odot$ and $R_2 \sim 6\,R_\odot$. These values are up to 30 per cent lower than those calibrated by Martins et al. (2005). This fact has already been shown by Fernández Lajús (2006): he analysed a sample of detached eclipsing binaries, the components of which are O-type stars lying near the ZAMS, i.e. V662 Car (= FO15), V572 Car and V731 Car (= CPD −59 2635). The same feature was found by Vaz et al. (1997, for HD 165921) and by Freyhammer et al. (2001, for V573 Car = CPD −59 2628).

Furthermore, assuming this inclination and the radii of the components calculated with our models, from our orbital solution we obtain rotational periods of 2.0 and 1.8 d. It seems, therefore, that rotation is not synchronized with orbital motion ($P \approx 2.96$ d). We plan to address this question in a future work, once we have studied the apsidal motion of our entire sample of systems.

Considering that the system is composed of two massive stars orbiting in a ∼3 d period, we explored the possibility of their being in contact. Thus we calculated $R_1/a_1 = 0.47$ and $R_2/a_2 = 0.40$ and compared these with the actual effective radii of their Roche lobes R_L (using the formula given in Eggleton 1983), which resulted in $R_{L,1}/a_1 = 0.75$ and $R_{L,2}/a_2 = 0.67$. Therefore the stars are within their respective Roche lobes.

Table 5. Age determinations of NGC 6530.

Ref.	$V_0 - M_v$	R	$\langle E(B-V)\rangle$	Age (Myr)
VA72	11.25	3.0	0.35	2
K77	10.7	3.0	0.35 ± 0.01	1–3
B84	11.5	3.2		$\sim 5 \pm 2$
S00	11.25 ± 0.1		0.35	1–2
D04				0.8
P05	$\simeq 10.48$		0.35	2.3
M08	10.15–10.44		0.32	2

R: ratio of total to selective absorption.
References: VA72: van Altena & Jones (1972); K77: Kilambi (1977); B84: Boehm-Vitense et al. (1984); S00: Sung et al. (2000); D04: Damiani et al. (2004); P05: Prisinzano et al. (2005); M08: Mayne & Naylor (2008).

3.7 On the age, distance and luminosity of HD 165052

As we have seen (Section 3.6), the method described in B02 is particularly sensitive to the age of the binary system. In fact, the age of both stars is the parameter that introduces the largest uncertainty in the calculation of the masses. Quite fortunately, HD 165052 belongs to the open cluster NGC 6530. Thus, it is natural to consider that HD 165052 has the age of NGC 6530. In Table 5 we summarize the age determinations found in the literature and the main related parameters.

Based on the theoretical gravitational contraction isochrones of Iben (1965), van Altena & Jones (1972) determined an age of 2 Myr for the cluster. Kilambi (1977), using *UBV* photographic photometry, estimated an age range of 1–3 Myr for most of the stars in the gravitational contraction stage. Boehm-Vitense, Hodge & Boggs (1984), studying *IUE* spectra of the O–B stars and using theoretical evolutionary tracks, inferred an age of $\sim 5 \pm 2$ Myr. Sung, Chun & Bessell (2000) obtained *UBVRI* and Hα photometry of the cluster and, by comparing it with evolutionary models, determined that the age of the most massive stars in the cluster is 1–2 Myr. Damiani et al. (2004) identified X-ray sources in the cluster as 0.5–1.5 Myr age pre-main-sequence stars with masses down to 0.5–1.5 $M_\odot$ and found evidence of an age gradient from north-west to south. The median age of stars in the central region of the cluster they have found was 0.8 Myr. Prisinzano et al. (2005) presented *BVI* photometry of the cluster and, using evolutionary tracks, found a median age of about 2.3 Myr. The most recent determination of the age of NGC 6530 is that of Mayne & Naylor (2008), who gave a nominal value of 2 Myr from fitting main-sequence models to data from literature sources. On the other hand, L07 calculated that the circularization time of this system should be less than 33 500 yr, but it is still eccentric; it should therefore be very young (or else its eccentricity is due to another physical process).

For our calculations we have assumed that the age of HD 165052 lies between 1 and 2 Myr. Thus, we have employed a value of 1.5 Myr with an error range of 0.5 Myr. This assumption is mainly supported by the works of Sung et al. (2000) and Mayne & Naylor (2008).

It is worth mentioning that, apart from the works quoted above, other authors have determined the distance to NGC 6530 (see Prisinzano et al. 2005, table 1 and references therein) or the absolute magnitude of the system. Using these data, assuming the standard ratio of total to selective absorption $R = 3.1$ (whenever the authors did not estimate another value) and the bolometric corrections given by Martins et al. (2005, table 4) for the binary component

spectral types, we have calculated the intrinsic luminosity of each component. To do this, we have assumed $V = 6.87 \pm 0.01$, which is the mean value of the photometric measurements reported in the SIMBAD data base, and we have considered that the luminosity ratio L_2/L_1 could be taken from the Martins et al. (2005, table 4) observational calibration.

In this way, we have obtained $4.8 < \log(L_1/L_\odot) < 5.5$. The lower value corresponds to the distance modulus $m - M = 10.34$ and colour excess $E(B-V) = 0.32$ determined by Mayne & Naylor (2008).[6] The upper value corresponds to $M_V = -4.8$ from Buscombe (1969). These data are represented by the extremes of the vertical error bars in the H–R diagram in Fig. 3. The horizontal error bars were traced at a luminosity level corresponding to the simple average of all the published photometric data. For the secondary star, we obtained $4.7 < \log(L_2/L_\odot) < 5.4$. The large range in our luminosity estimations arises from the differences between the distance moduli adopted by different authors.

In order to include the binary components in Fig. 3, we have assigned to each one the $T_{\rm eff}$ from the observational calibration of Martins et al. (2005, table 4) for its spectral type. The horizontal bar lengths indicate the dispersion calculated in the same work.

4 SUMMARY

We have observed the spectroscopic binary HD 165052 by gathering a set of high-resolution and high signal-to-noise ratio spectra, from which we have measured the radial velocity of its components over its orbital movement. With these data we have determined the parameters of its current orbit, confirming that it is eccentric, as has been realized by Arias et al. (2002). Re-analysing all the previously published radial velocity measurements together, we have demonstrated the precession of the orbit, a fact suggested by A02. We have also determined for the first time the apsidal motion rate of the system, $\dot{\varpi} = 0.0331 \pm 0.0009$ day^{-1}, which seems to be the highest value ever measured in an O+O binary system.

We have disentangled the component spectra and re-classified them, finding that both present the *z* spectral feature. Thus, we classify the primary as O7V*z* and the secondary as O7.5V*z*.

Using the apsidal motion rate, with the method described in Benvenuto et al. (2002), we have calculated the absolute masses of the binary components ($M_1 = 22.5 \pm 1.0\,M_\odot$, $M_2 = 20.5 \pm 0.9\,M_\odot$). These masses lie close to those determined for eclipsing binaries of the same spectral types and compare well with those theoretically estimated in the Martins et al. (2005) calibration.

We have estimated the luminosities of the binary components, but unfortunately there is a large uncertainty in these calculations because of the large differences in the distances previously determined to the cluster NGC 6530. This is why the masses estimated from photometry and evolutionary models are very uncertain. Nonetheless, the masses that we have obtained from the apsidal motion rate suggested that the distance to the cluster could be around the smallest determined until now. To solve this apparent inconsistency, it is necessary to have new independent determinations of the distance to the cluster.

ACKNOWLEDGEMENTS

We acknowledge our referee, Ian Howarth, for his very useful comments, which improved this paper substantially.

We are very grateful to Nidia Morrell and Rodolfo Barbá for their kind collaboration in the acquisition of the spectra at Las Campanas and ESO–La Silla observatories. We also acknowledge Petr Hadrava for kindly allowing us to use the FOTEL code.

We thank the directors and staff of CASLEO, LCO and ESO, La Silla, for the use of their facilities and their gentle hospitality during the observing runs.

This research has made use of NASA's Astrophysics Data System and the SIMBAD data base, operated at CDS, Strasbourg, France.

This work is based on observations made with three facilities: the J. Sahade telescope at Complejo Astronómico El Leoncito (CASLEO), the du Pont telescope at Las Campanas Observatory (LCO) and the 2.2-m telescope at La Silla Observatory (ESO) under programmes ID 083.D-0589 and 087.D-0946.

[6] Actually, Mayne & Naylor (2008) report in one of their fits (their table 8) $10.15 < m - M < 10.44$, with a nominal value 10.34.

REFERENCES

Andersen J. et al., 1985, A&AS, 59, 15
Arias J. I., Morrell N. I., Barbá R. H., Bosch G. L., Grosso M., Corcoran M., 2002, MNRAS, 333, 202 (A02)
Barbá R. H., Gamen R., Arias J. I., Morrell N., Maíz Apellániz J., Alfaro E., Walborn N., Sota A., 2010, Rev. Mex. Astron. Astrofis. Ser. Conf., 38, 30
Benvenuto O. G., De Vito M. A., 2003, MNRAS, 342, 50
Benvenuto O. G., Serenelli A. M., Althaus L. G., Barbá R. H., Morrell N. I., 2002, MNRAS, 330, 435 (B02)
Bertiau F. C., Grobben J., 1969, Ric. Astron. Sp. Vaticana, 8, 1
Boehm-Vitense E., Hodge P., Boggs D., 1984, ApJ, 287, 825
Bulut I., Demircan O., 2007, MNRAS, 378, 179
Buscombe W., 1969, MNRAS, 144, 31
Claret A., 1999, A&A, 350, 56
Claret A., Gimenez A., 1991, A&AS, 87, 507
Collins G. W., II, 1974, ApJ, 191, 157
Conti P. S., 1974, ApJ, 187, 539
Conti P. S., Leep E. M., Lorre J. J., 1977, ApJ, 214, 759
Damiani F., Flaccomio E., Micela G., Sciortino S., Harnden F. R., Jr, Murray S. S., 2004, ApJ, 608, 781
de Jager C., Nieuwenhuijzen H., van der Hucht K. A., 1988, A&AS, 72, 259
Demarque P., Woo J.-H., Kim Y.-C., Yi S. K., 2004, ApJS, 155, 667
Dimitrijevic M. S., Sahal-Brechot S., 1990, A&AS, 82, 519
Eggleton P. P., 1983, ApJ, 268, 368
Fernández Lajús E., 2006, PhD thesis, Univ. Nac. de La Plata, Argentina
Freyhammer L. M., Clausen J. V., Arentoft T., Sterken C., 2001, A&A, 369, 561
González J. F., Levato H., 2006, A&A, 448, 283
Hadrava P., 2004, Publ. Astron. Inst. Acad. Sci. Czech Rep., 92, 1
Hayford P., 1932, Lick Obs. Bull., 16, 53
Iben I., Jr, 1965, ApJ, 141, 993
Jeffery C. S., 1984, MNRAS, 207, 323
Kilambi G. C., 1977, MNRAS, 178, 423
Lanz T., Hubeny I., 2003, ApJS, 146, 417
Levi-Civita T., 1937, Am. J. Math., 59, 225
Linder N., Rauw G., Sana H., De Becker M., Gosset E., 2007, A&A, 474, 193 (L07)
Maíz Apellániz J., Sota A., Walborn N. R., Alfaro E. J., Barbá R. H., Morrell N. I., Gamen R. C., Arias J. I., 2011, Highlights of Spanish Astrophysics, VI, 467
Martins F., Schaerer D., Hillier D. J., 2005, A&A, 436, 1049
Massey P., Morrell N. I., Neugent K. F., Penny L. R., DeGioia-Eastwood K., Gies D. R., 2012, ApJ, 748, 96
Mayne N. J., Naylor T., 2008, MNRAS, 386, 261
Morrison N. D., Conti P. S., 1978, ApJ, 224, 558 (M78)
Petrova A. V., Orlov V. V., 1999, AJ, 117, 587
Plaskett J., 1924, Publ. DAO, 2, 286
Prisinzano L., Damiani F., Micela G., Sciortino S., 2005, A&A, 430, 941
Sanford R. F., 1949, ApJ, 110, 117

Slettebak A., Collins G. W., II, Parkinson T. D., Boyce P. B., White N. M., 1975, ApJS, 29, 137
Sota A., Maíz Apellániz J., Walborn N. R., Alfaro E. J., Barbá R. H., Morrell N. I., Gamen R. C., Arias J. I., 2011, ApJS, 193, 24
Sterne T. E., 1939, MNRAS, 99, 451
Stickland D. J., Lloyd C., Koch R. H., 1997, Observatory, 117, 295 (S97)
Sung H., Chun M., Bessell M., 2000, AJ, 120, 333
Thome J. M., 1892, Resultados del Observatorio Nacional Argentino, 16, 1
van Altena W. F., Jones B. F., 1972, A&A, 20, 425
Vaz L. P. R., Cunha N. C. S., Vieira E. F., Myrrha M. L. M., 1997, A&A, 327, 1094
Walborn N. R., 2009, STScI Symp. Ser., 20, 167
Wilson R. E., 1953, General Catalogue of Stellar Radial Velocities. Carnegie Inst., Washington, DC

APPENDIX A: DISENTANGLED SPECTRA

Fig. A1 compares the primary and secondary star spectra of HD 165052, resampled to $R \sim 2500$, with those of spectral standards HD 93146 and HDE 319703 A.

APPENDIX B: TABLES OF RADIAL VELOCITIES

Table B1 lists the radial velocities of HD 165052 previously reported in the literature. Table B2 gives the radial velocity measurements of individual lines.

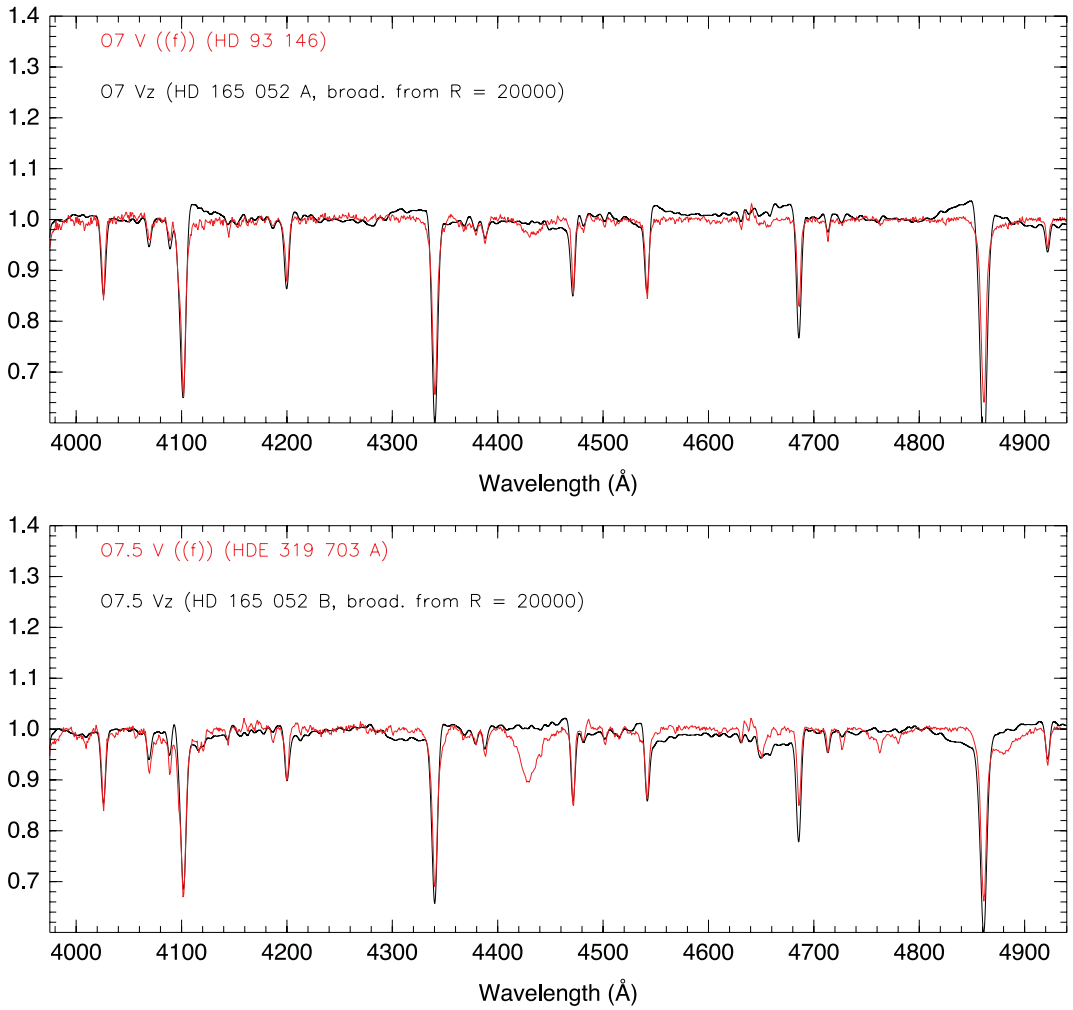

Figure A1. HD 165052 primary (A) and secondary (B) star spectra resampled to $R \sim 2500$ (black), compared with those of the spectral standards HD 93146 and HDE 319703 A (red in the online article). Note the greater intensity of the He II λ4686 absorption line (the *z* feature). The difference between the continuum level in the bluer and redder wings of some lines is due to an artefact of the disentangling algorithm. The figure was generated with the MGB code (Sota et al. 2011).

Table B1. Radial velocities of HD 165052 previously reported.

HJD −240 0000	v_1	v_s	v_2	Ref.
∼24000		3.0		P24
25371.99		6.0		H32
∼33000		-1.0 ± 8.0		S49
∼35000		3.0 ± 2.5		W53
40075.70		-6.6 ± 3.2		C77
40047.80		-3.1 ± 4.5		C77
42560.940		−9		M78
42561.858		1		M78
42562.921	−73		93	M78
42565.822	−106		95	M78
42566.850		1		M78
42687.587		12		M78
42688.588	103		−121	M78
42689.591	−91		62	M78
42691.584	100		−94	M78
42937.771	−63		64	M78
42938.861		−1		M78
42939.800	101		−111	M78
42940.918	−81		88	M78
42941.851		5		M78
42942.902	74		−96	M78
42943.863	−61		91	M78
43089.575		11		M78
43090.573	110		−105	M78
43091.579	−66		101	M78
43092.571		10		M78
44121.777	99.2		−109.8	S97
44459.983	−83.4		98.4	S97
44899.113	90.9		−105.5	S97
45123.793	89.6		−86.7	S97
48864.018	39.0		−42.9	S97
48864.053	47.0		−48.4	S97
48867.621	100.0		−91.8	S97
49101.414	54.7		−67.9	S97
49399.573	86.7		−99.5	S97
49817.685	−100.1		106.9	S97
49818.419	13.5		−25.3	S97
49818.842	79.4		−100.0	S97
49819.417	61.0		−79.5	S97
49821.120	−50.2		38.6	S97
49965.110	−72.5		87.8	S97
49854.640	88.2		−98.5	A02
49931.634	69.2		−91.4	A02
49932.663	−76.5		95.4	A02
49934.577	75.2		−82.8	A02
49935.605	−77.6		88.5	A02
49937.587	71.9		−73.2	A02
50239.906	−74.0		76.8	A02
50241.823	82.5		−90.9	A02
50244.902	72.6		−76.5	A02
50245.857	−74.7		82.5	A02
50293.763	−74.5		82.6	A02
50296.787	−63.2		64.3	A02

Table B1 – *continued*

HJD −240 0000	v_1	v_s	v_2	Ref.
50671.471	−78.1		94.0	A02
51299.7250	88.3		−100.8	L07
51300.7319	−56.5		76.9	L07
51300.9264	−86.7		96.6	L07
51301.9281	31.2		−24.9	L07
51304.7434	7.4		−1.7	L07
51304.7507	15.0		−12.5	L07
51304.9309	40.1		−39.5	L07
51323.8361	17.9		−25.8	L07
51327.6014	−87.7		106.8	L07
51327.9127	−93.7		103.3	L07
51670.7601	−80.1		103.7	L07
51671.7225	96.3		−111.3	L07
51672.7016	−15.9		28.7	L07
51714.835	−87.2		102.9	A02
51714.862	−93.5		99.2	A02
51715.796	61.2		−62.9	A02
51716.570	71.6		−68.5	A02
51716.656	34.0		−41.9	A02
51717.609	−80.7		95.6	A02
51717.727	−90.5		95.3	A02
51717.829	−93.0		97.7	A02
52066.791	−70.1		90.6	A02
52067.768	95.6		−110.5	A02
52069.730	−75.4		86.6	A02
52069.794	−67.3		76.2	A02
52070.621	93.3		−97.1	A02
52070.731	103.5		−104.9	A02
52070.792	102.8		−107.4	A02
52072.663	−75.3		90.1	A02
52072.717	−69.4		78.9	A02
52335.8879	−41.0		56.9	L07
52336.8791	97.5		−118.5	L07
52337.8880	−54.9		70.1	L07
52338.8808	−46.1		47.8	L07
52339.8848	96.9		−111.2	L07
52381.8324	6.6		−5.7	L07
52382.8569	−79.7		103.3	L07
52383.8577	95.4		−103.1	L07

Notes. v_s: systemic velocity.

Refs: H32: Hayford (1932); C77: Conti, Leep & Lorre (1977); L07: Linder et al. (2007); M78: Morrison & Conti (1978); P24: Plaskett (1924); S49: Sanford (1949); S97: Stickland et al. (1997); W53: Wilson (1953); A02: Arias et al. (2002).

Table B2. Radial velocity measurements for HD 165052.

HJD	Phase	v_r			He I		He I		Si IV		He II		He I		He I		Mg II	
−245 0000		mean			3819		4026		4088		4200		4387		4471		4481	
	ϕ	(km s^{-1})																
		1	2		1	2	1	2	1	2	1	2	1	2	1	2	1	2
4582.8675	0.86	97.1	−108.8		102.9	−98.7	103.8	−101.0	90.7	−104.2	122.6	−100.9	105.3	−106.5	85.8	−112.9	95.6	−116.3
4693.6231	0.34	−81.6	91.7		−67.7	90.8	−81.3	94.4	−94.2	96.1	−59.9	119.6	−75.8	100.6	−85.3	87.4	−82.1	73.7
4695.6483	0.03	13.8	−8.8	*	28.4	−12.6	23.0	−1.9	−2.9	−11.5	47.3	−25.2	40.0	−29.6	14.4	−11.8	16.3	–
4696.5568	0.34	−85.4	95.1		−58.4	98.1	−80.2	100.4	−88.4	87.8	−85.2	99.7	−77.8	95.9	−92.8	87.4	−92.8	96.7
4696.6286	0.36	−80.2	94.3		−77.1	91.5	−66.9	108.0	−79.2	86.1	−68.9	113.4	−74.1	97.0	−83.9	94.3	−78.5	88.4
4696.6605	0.37	−76.8	91.4		−57.1	99.4	−82.1	97.8	−76.8	85.7	−72.4	102.1	–	–	−80.5	80.8	−88.5	97.6
4697.6220	0.70	73.7	−76.1		65.4	–	–	−84.6	62.0	−80.3	69.7	–	–	−73.9	–	−72.7	57.0	−84.7
4955.8004	0.07	−7.6	5.1	*	36.7	1.8	6.6	15.7	−12.6	8.4	−12.9	–	−12.3	−11.1	−8.5	6.1	−9.7	9.5
4956.9100	0.44	−57.5	61.0		−36.7	75.1	−49.3	65.3	−53.3	72.9	−60.9	62.3	−46.8	71.9	−59.3	59.7	−71.4	51.2
4964.8865	0.14	−57.6	66.7		−26.5	86.2	−57.1	67.4	−60.4	72.6	−86.9	79.7	−50.4	75.3	−61.2	59.6	−78.7	85.7
4965.8323	0.46	−47.1	57.4		−21.1	68.9	−34.1	64.8	−58.2	60.3	−70.9	63.7	−45.6	64.0	−44.5	56.9	–	26.0
4966.8550	0.81	100.8	−106.1		101.0	−92.8	101.9	−106.0	100.9	−105.9	96.6	−119.2	114.1	−115.1	96.9	−110.5	–	–
4967.8220	0.13	−56.1	62.9		−19.1	71.9	−55.4	61.6	−52.9	66.5	−75.0	91.0	−89.5	40.1	−63.6	57.4	−61.2	87.1
4968.8723	0.49	−38.8	40.6		−19.6	41.6	−33.8	42.9	−37.5	38.8	−58.1	55.6	−21.9	48.9	−42.3	31.9	−44.8	41.8
5046.6533	0.81	103.7	−109.9		108.9	−107.0	106.4	−108.3	108.0	−104.3	115.4	−92.8	103.5	−110.8	98.6	−117.5	93.5	−130.4
5047.7305	0.17	−73.8	81.8		−54.1	91.8	−68.3	86.3	−71.4	79.6	−64.0	83.4	−31.4	104.4	−82.1	70.9	−47.4	103.5
5048.7185	0.51	−24.7	29.3	*	−12.9	34.6	−31.8	35.1	−29.4	34.6	−23.5	33.4	−19.9	41.4	−23.3	24.5	92.8	89.8
5049.7159	0.85	106.4	−106.5		97.1	−109.1	108.0	−108.2	107.6	−106.1	104.6	−114.7	69.2	−102.1	115.1	−109.3	107.8	−120.2
5052.7320	0.87	100.6	−104.9		101.4	−105.3	98.5	−100.0	100.1	−105.6	100.1	−98.0	101.2	−104.9	93.5	−109.9	111.4	−105.7
5337.6475	0.28	−94.3	101.3		−87.7	120.3	−106.9	93.6	−79.7	105.3	−106.1	99.9	−114.5	–	−99.6	101.7	−77.3	112.8
5339.7307	0.99	38.0	−45.7		–	−44.2	40.9	−56.4	48.3	−41.3	–	–	46.4	−59.7	37.8	−53.9	–	−54.7
5340.6327	0.29	−94.6	100.7		−88.1	120.6	−108.7	96.8	−85.9	106.6	−98.0	84.1	−110.2	131.0	−99.5	100.7	−109.9	–
5341.5812	0.61	26.5	−27.4	*	73.7	−27.9	35.6	−31.7	35.1	−27.5	36.9	−45.5	46.1	−56.6	20.9	−30.6	27.9	−56.7
5342.6292	0.97	54.0	−60.9		81.7	−46.2	43.4	−78.0	60.1	−56.2	64.4	−68.7	27.0	−87.9	49.9	−68.1	56.0	−72.1
5376.5522	0.45	−52.2	59.9		−21.9	73.4	−43.2	69.7	−60.7	62.3	−48.3	78.6	−49.7	61.4	−52.1	58.7	−33.6	76.2
5378.7551	0.19	−79.7	88.5		−55.7	92.7	−63.1	100.6	−92.2	83.8	−81.2	72.6	−71.2	76.9	−82.6	83.0	−60.6	112.8
5380.5253	0.79	97.3	−106.1		110.7	−93.7	93.4	−110.3	91.2	−108.3	90.4	−116.3	103.6	−92.3	106.0	−110.2	83.5	−98.5
5381.7473	0.21	−84.7	93.2		−63.2	100.2	−75.4	101.3	−85.0	100.3	−84.4	85.5	−66.8	87.8	−81.4	96.8	−73.0	91.5
5383.7515	0.88	91.5	−98.5		90.5	−91.9	98.4	−97.5	95.0	−99.9	97.2	−98.2	96.5	−88.5	93.5	−102.0	79.0	−87.1
5429.6974	0.43	−57.0	70.1		−26.1	88.4	−46.1	69.9	−67.0	71.8	−60.4	64.2	−77.6	57.0	−49.6	72.8	−68.0	–
5430.6168	0.74	87.8	−91.7		75.4	−91.3	84.1	−96.8	89.0	−94.0	84.8	−99.1	101.1	−84.8	95.8	−89.5	67.9	−86.6
5431.6959	0.11	−42.6	51.3		−22.1	55.3	−37.1	53.0	−59.1	47.0	−40.4	49.7	−19.4	72.3	−34.4	54.3	–	56.2
5432.6362	0.43	−58.1	69.5		−25.4	86.4	−57.8	67.8	−66.1	66.6	−70.0	59.7	−43.8	79.6	−53.7	69.7	−45.0	77.4
5433.5059	0.72	81.0	−88.3		97.8	−73.1	69.8	−89.1	85.9	−91.5	57.4	−125.4	82.4	−89.9	88.7	−83.4	64.3	−79.0
5434.6834	0.12	−46.7	61.2		−5.3	80.4	−51.0	58.3	−62.2	55.1	−35.0	67.9	−36.2	66.4	−42.1	61.7	−65.9	47.4
5435.5627	0.42	−65.0	74.0		−28.6	87.6	−60.6	70.8	−71.4	74.6	−81.0	79.4	−81.5	56.4	−60.3	76.5	−67.3	50.3
5698.8397	0.51	−6.0	41.2	*	–	–	1.6	43.3	−5.4	46.5	−15.3	51.5	3.8	55.2	−3.7	38.5	−14.8	39.1

Table B2 – *continued*

He II 4542		He II 4686		He I 4713		He I 4921		He I 5015		He II 5411		O III 5592		C IV 5801		C IV 5812		He I 5875	
1	2	1	2	1	2	1	2	1	2	1	2	1	2	1	2	1	2	1	2
89.0	−119.5	99.6	−103.9	98.0	−100.4	97.6	−109.4	90.1	−105.8	102.1	−100.9	101.1	−108.3	92.6	−97.6	96.0	−107.6	97.8	−114.4
−82.6	68.2	−83.4	95.8	−90.2	96.2	−60.1	99.7	−84.7	79.4	−81.1	93.9	−88.6	80.7	−79.1	90.6	−96.9	82.1	−82.1	94.5
9.3	−5.2	–	0.4	16.3	−18.9	11.9	−20.2	20.2	−6.6	6.0	−11.9	12.2	−9.6	5.0	−17.8	23.5	−23.4	10.3	−5.9
−92.0	85.0	−81.3	100.6	−79.9	93.7	−79.6	85.2	−75.2	98.2	−86.5	97.6	−88.1	93.8	−76.5	96.7	−93.3	86.5	−88.1	98.1
−91.6	82.6	−79.8	86.6	−80.8	96.8	−71.4	94.6	−82.9	83.9	−80.5	95.9	−79.9	93.7	−76.1	94.3	−95.2	–	−82.5	95.5
−87.8	87.5	−72.0	95.6	−84.4	89.8	−72.2	90.5	−73.2	91.3	−71.6	102.0	−82.3	84.8	−68.7	88.4	−88.2	82.6	−78.6	90.5
–	–	59.1	−75.8	–	−68.8	–	–	–	−78.7	–	–	71.9	−70.9	55.3	–	–	–	–	−69.4
−2.1	−15.4	−12.1	9.6	−16.8	14.5	2.8	19.7	−5.2	18.4	–	24.0	−13.0	9.7	−20.7	10.1	−29.6	20.2	−1.9	12.8
−56.3	43.0	−56.9	64.8	−64.5	60.4	−54.6	69.4	−58.7	65.1	−69.3	56.2	−57.5	66.6	−50.5	64.6	−67.3	50.9	−56.1	61.2
−58.7	58.3	−53.8	68.2	−68.6	66.8	−47.9	68.9	−45.9	71.6	−59.0	65.8	−55.4	69.5	−49.6	71.2	−66.2	56.4	−58.3	64.9
−46.1	41.6	−44.0	58.8	−58.8	63.2	−46.1	54.5	−28.6	74.6	−52.4	54.5	−51.4	57.8	−50.0	53.2	−55.8	48.2	−49.9	53.7
106.4	−95.5	103.0	−100.6	107.1	−119.6	99.7	−109.0	85.7	−113.1	100.0	−94.0	98.5	−110.5	100.2	−102.4	95.0	−102.9	105.6	−113.3
−56.2	60.8	−52.6	60.9	−39.9	76.0	−39.2	78.2	−62.9	60.5	−57.6	57.2	−55.1	66.8	−52.7	57.6	−58.0	56.7	−55.2	62.4
−42.2	38.2	−35.9	40.1	−35.3	47.4	−44.5	38.5	−32.5	48.1	−40.5	37.5	−41.5	39.6	−41.2	32.7	−43.5	37.3	−36.1	41.9
114.6	−100.4	98.9	−110.8	94.4	−106.4	95.6	−118.8	89.5	−113.1	103.8	−113.2	100.9	−107.5	101.0	−103.1	105.8	−106.9	103.3	−109.5
−74.6	96.3	−78.6	82.7	−70.2	77.0	−68.0	87.6	−78.6	76.1	−77.5	74.5	−66.4	85.2	−60.9	79.8	−86.3	86.7	−70.6	82.7
−35.2	28.8	−25.4	28.6	−4.3	16.3	−30.3	22.1	−22.7	28.0	−32.7	41.5	−30.7	33.3	−29.8	23.7	−47.1	29.8	−20.3	27.8
115.3	−100.3	103.5	−105.4	100.7	−105.8	101.9	−109.4	96.4	−109.7	94.2	−112.9	104.9	−107.9	93.2	−95.2	100.9	−107.6	108.5	−106.6
93.4	−93.2	104.8	−110.5	99.1	−110.4	106.2	−111.5	84.9	−102.4	101.1	−97.9	102.6	−106.2	92.8	−94.4	108.8	−98.4	102.2	−105.9
−89.5	86.2	−91.0	106.3	−95.5	98.1	−95.4	104.5	−93.7	87.0	−92.5	96.7	−97.5	105.7	−91.9	102.7	−86.8	102.2	−95.3	100.0
42.4	−48.9	40.7	−41.5	37.2	−51.3	51.1	−52.1	46.5	−47.5	53.4	–	–	–	–	–	–	–	–	–
−96.7	80.4	−97.5	102.0	−95.7	99.5	−89.1	104.8	−94.3	95.7	−87.6	101.3	−99.5	102.6	−90.0	101.2	−82.4	101.1	−93.7	101.5
30.4	−33.8	24.5	−23.6	22.6	−31.2	30.0	−33.5	30.0	−30.0	19.6	−17.6	25.2	−30.7	7.3	−31.8	30.2	−29.8	21.3	−22.7
58.3	−56.4	55.5	−54.2	51.8	−66.2	68.7	−58.5	50.9	−65.9	51.9	−52.6	54.2	−65.3	–	−58.3	48.8	−70.6	50.9	−59.1
−65.2	52.9	−54.3	60.6	–	55.7	−63.9	47.0	−64.4	48.4	−52.3	57.9	−55.5	60.4	−56.7	48.1	−67.4	47.6	−47.0	55.4
−73.1	85.7	−87.4	94.7	−75.8	92.2	−97.9	84.9	−88.5	85.0	−80.3	87.5	−82.8	91.7	−76.0	89.0	−76.7	96.8	−73.1	91.9
94.5	−106.4	99.8	−106.4	81.4	−100.7	76.7	−119.3	88.6	−107.4	92.5	−94.6	99.4	−111.8	87.9	−94.7	103.4	−102.6	100.4	−103.6
−97.6	84.0	−91.7	94.1	−92.8	85.2	−97.8	84.1	−83.3	77.0	−86.0	86.0	−84.6	90.9	−78.0	95.5	−88.0	93.9	−79.5	97.8
86.5	−99.9	89.8	−101.2	95.6	−106.7	90.7	−103.2	78.8	−103.3	92.0	−85.3	91.6	−99.8	81.8	–	88.8	−101.7	93.3	−97.3
−67.8	69.0	−59.0	76.9	−63.6	65.7	−54.1	64.8	−66.4	69.7	−68.5	56.8	−57.9	68.7	−52.1	65.4	−52.0	68.5	−52.5	68.8
88.6	−109.0	88.1	−92.7	84.3	−91.3	90.3	−93.3	87.3	−95.3	89.1	−72.0	87.8	−93.3	81.9	−84.3	99.8	−81.2	87.3	−94.0
−54.9	43.1	−40.3	55.6	−55.8	39.9	−54.5	44.1	−40.2	55.8	−56.5	43.3	−43.9	52.2	−38.3	48.3	−42.2	55.0	−37.6	51.8
−60.5	65.4	−56.8	76.5	–	65.7	−68.6	59.6	−62.5	59.8	−53.6	71.7	−62.3	66.3	−55.6	71.5	−54.1	65.5	−58.6	66.3
83.8	−81.7	77.6	−93.5	83.7	−99.7	96.2	−88.5	81.4	−88.3	80.8	−87.0	73.1	−94.3	66.3	–	64.2	−99.1	83.9	−82.4
−52.8	63.6	−43.7	61.5	–	–	−58.4	52.0	−54.8	55.3	−52.6	55.5	−39.3	62.9	−44.2	60.0	−42.2	56.4	−45.5	59.8
−70.5	76.4	−63.1	83.6	−66.1	75.9	−69.8	65.4	−63.3	70.4	−69.1	63.9	−66.0	74.6	−51.8	75.8	−60.4	66.8	−65.6	70.2
0.6	16.5	−8.2	42.8	−3.1	39.9	0.1	41.9	−2.7	42.0	−27.2	46.4	−10.8	44.8	−12.8	35.4	−26.2	40.6	−2.4	42.2

Notes.

*: One-tenth weight assigned in orbital solution fit because of strong lines blending.

−: Cross-correlation does not provide a reliable measurement.

This paper has been typeset from a TEX/LATEX file prepared by the author.